APPLICATION OF THE VOF METHODOLOGY FOR THE ANALYSIS OF TRANSIENT SHEAR RATES IN DROPLET-WALL INTERACTION

Roesler, S.*, Domnick, J., Ludwig, M., Ocak, B. and Hildenbrand, S.
*Author for correspondence
Department of Mechanical Engineering,
Hochschule Esslingen
Kanalstrasse 33
D-73728 Esslingen, Germany
E-mail: stefan.roesler@hs-esslingen.de

ABSTRACT

Sprays are very frequently utilized for the generation of an evenly distributed liquid film on a surface, e.g. in finishing or coating applications. The process liquids in this context usually exhibit a non-Newtonian behaviour, i.e. shear-thinning characteristics plus thixotropy. In order to be able to predict the flow inside the developing liquid film, the local instantaneous viscosities of the fluid need to be available, which are primarily influenced by the viscosity of the droplets deposited on the film surface. For shear-thinning liquids, this viscosity depends upon the transient shear rates occurring during the droplet-wall or better droplet-film interaction.

The present paper describes activities applying the VOF methodology to predict the local instantaneous shear rates of droplet-wall interaction in a relevant range of Weber numbers.

NOMENCLATURE

A	[-]	Splash onset coefficient
C_1	[-]	Constant in power law correlation
C_2	[-]	Constant in power law correlation
Co	[-]	Courant number
$Dv(10)$	[m]	10%-quantile of measured droplet diameters
$Dv(50)$	[m]	50%-quantile (median) of measured droplet diameters
$Dv(90)$	[m]	90%-quantile of measured droplet diameters
d	[-]	Droplet diameter
k	[-]	Constant in Herschel-Bulkley law
La	[-]	Laplace number
n	[-]	Constant in Herschel-Bulkley law
s	[1/m³s]	Phase volume fraction source term
S	[m²]	Surface area
v	[m/s]	Velocity
V	[m³]	Volume
We	[-]	Weber number
α_i	[-]	Volume fraction of phase i
$\dot{\gamma}$	[1/s]	Shear rate
δ	[m]	Liquid film thickness
μ	[Pas]	Dynamic viscosity
ρ	[kg/m³]	Density
σ	[N/m]	Surface tension
τ_0	[Pa]	Yield stress
Δt	[s]	Time step size
Δx	[m]	Cell size

INTRODUCTION

Increasingly shorter cycle times in product development, e.g. in the automotive industry have considerably supported the application of simulation techniques in a large number of areas. The production and availability of hardware prototypes has been reduced correspondingly. One range of processes relying largely upon testing and expert experience in the past is surface coating and finishing. The reduced availability of prototypes and the considerable advances in simulation software techniques and computer hardware have pushed the development of CAE techniques also in this field over the last years [1], [2].

In automobile body cavity conservation due to the complexity of the physical phenomena numerical simulation techniques are only starting to evolve. The goal of the process itself is to cover cavities in automobile bodies like rocker panels with a corrosion protection layer which usually consists of a wax-based substance. The substance is sprayed from nozzles inserted into the cavities onto the inner surfaces forming a liquid film which subsequently starts to move due to gravity and solidifies. The main challenges are to guarantee sufficient corrosion protection at a minimum material input and a minimum of nozzle positions. A numerical technique to realistically simulate this process needs to account for the following phenomena:

- Primary breakup of liquid in spray nozzle
- Flow of spray in the cavity
- Droplet-wall interaction
- Generation of liquid film
- Non-Newtonian flow of liquid film
- Solidification

While the flow of the spray inside the cavity can be modelled using standard Euler/Lagrange techniques, most of the other phenomena associated with the process are non-trivial to include into a simulation framework. The present paper focusses on the droplet-wall interaction process, which is of great importance for the generation and flow of the liquid film since the shear rates in the droplet and the film during the interaction process due to the non-Newtonian characteristics of

the liquid directly influence the local instantaneous viscosity in the film.

RHEOLOGICAL CHARACTERISTICS OF THE FLOW

The substances applied for body cavity preservation usually are either paraffin-like waxes or emulsions and exhibit shear-thinning and thixotropic rheological characteristics, i.e. under the effect of local shear, the viscosity of the liquid is reduced and after return to a non-shear condition the viscosity requires time to recover to its low shear value. The local dynamic viscosity according to the shear-thinning behaviour can be described e.g. by a simple power-law correlation

$$\mu(\dot{\gamma}) = C_1 \cdot \dot{\gamma}^{(C_2-1)}$$

or by a Herschel-Bulkley law

$$\mu(\dot{\gamma}) = \left(\frac{\tau_0}{\dot{\gamma}} + \left(k \cdot \dot{\gamma}^{(n-1)} \right) \right)$$

with the constants C_1 and C_2 or τ_0, k and n to be defined experimentally [3]. For the effect of thixotropy, various approaches are available [4]. In the frame of a CFD analysis, the most promising method is to implement an additional scalar transport equation for the viscosity with an adequate source term for shear-thinning and thixotropy.

In the flow system under consideration the liquid undergoes a first high-shear condition during the atomization process in the nozzle. It is assumed that the material reaches its equilibrium viscosity for very high shear rates. The subsequent droplet flow in the cavity happens under low shear rates, so that a viscosity recovery takes place. A second high-shear condition is given during the impingement of the droplet on the wall/liquid film. This local instantaneous viscosity defines the viscosity of the added mass in the liquid film due to the droplet deposition. In the film itself due to the moderate shear rates a second and enduring viscosity recovery occurs.

PRELIMINARY EXPERIMENTAL INVESTIGATION OF DROPLET PARAMETERS

In order to be able to investigate the droplet-wall interaction phenomena in a realistic area of Weber numbers, an experimental investigation of the spray properties under typical boundary conditions was carried out. The experimental setup consists of a commercial high-pressure metering pump for the liquid, an internal 0.4 mm diameter plain orifice pre-atomizer and a connected three-hole nozzle (outlet diameters 0.8 mm, 1.2 mm and 1.6 mm) with the holes arranged along one circumference of the nozzle body at an angular offset of 120°. The liquid under investigation is a standard conservation wax (so-called 100% wax) with a high-shear dynamic viscosity of 0.072 Pas and a density of 970 kg/m³.

Droplet sizes are measured using a laser diffractometer (Spraytec) of Malvern Instruments Ltd. The center of the cylindrically shaped probe volume (diameter 10 mm) is located approximately 10 mm from the nozzle exit. Therefore, the obtained volume weighted droplet size distributions represent integral data for the complete spray cone at this distance. The results of the measurements are shown in Fig. 1.

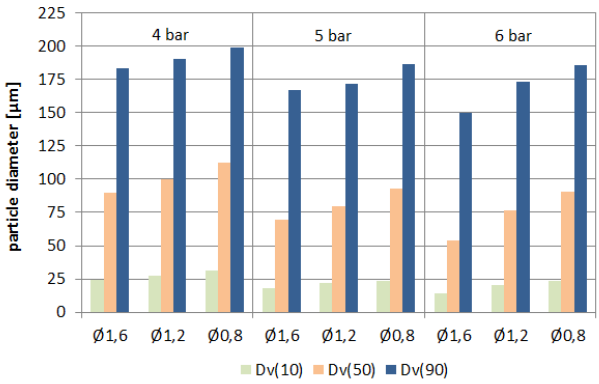

Fig. 1: Measured volume-averaged droplet diameters

The droplet velocities are measured by means of a Dantec 2D fibre optic based laser Doppler anemometer in back-scattering mode. Obtained velocity data in axial and radial spray direction are shown in Fig. 2.

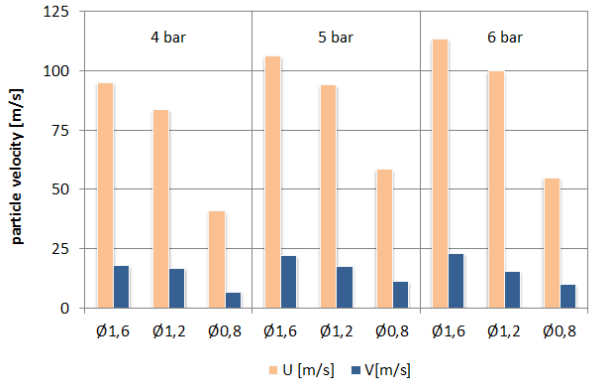

Fig. 2: Measured axial centerline (U) and radial (V) droplet velocities

The results present a very consistent picture. Droplet diameters Dv(10), Dv(50) and Dv(90) decrease with increasing upstream pressure and increasing hole diameter. The droplet diameters range from 15 µm to 150 µm for 1.6 mm hole diameter and 6 bar upstream pressure and from 30 µm to 200 µm for 0.8 mm hole diameter and 4 bar upstream pressure. The LDA data exhibit relatively high droplet velocities in axial direction. The velocities range from 40 m/s at 4 bar upstream pressure and 0.8 mm hole diameter to 113 m/s at 6 bar upstream pressure and 1.6 mm hole diameter. The radial velocities are considerably smaller (7 m/s to 23 m/s). The Weber numbers of the obtained experimental data

$$We = \rho \cdot v^2 \cdot d / \sigma$$

cover a range of 6000 < We < 26000.

VOF METHODOLOGY

The VOF methodology is a numerical technique for capturing a phase interface (usually gas-liquid, but also applicable for immiscible liquids) in the CFD analysis of multiphase flows and was first proposed by Hirt and Nichols in 1981 [5]. Today, VOF is a standard method in most commercial and open source CFD codes. The major advantage of the method is that it requires only one additional scalar transport equation for the phase volume fraction α_i to be solved compared to a single phase problem:

$$\frac{d}{dt}\int_V \alpha_i dV + \int_S \alpha_i v \cdot n dS = \int_V \left(s_{\alpha_i} - \frac{\alpha_i}{\rho_i}\frac{D\rho_i}{Dt} \right) dV$$

Details of the method can be found e.g. in [6]. In order to conserve sharp interfaces between the phases an adequate discretization scheme e.g. High Resolution Interface Capturing scheme (HRIC) has to be applied, which always requires comparably small Courant numbers

$$Co = v \cdot \Delta t / \Delta x$$

generally in the order of 0.25 < Co < 1. With the boundary conditions of high droplet velocities and small droplet diameters in the present investigation, the allowable time steps Δt will be extremely small generating considerable computational effort to perform the analyses.

SETUP OF COMPUTATIONAL DOMAIN AND CFD ANALYSES

The computational domain for the analyses has to include the droplet itself, the flow path of the droplet in the cavity and the wall area around the impinging droplet. In the frame of the present investigation the droplet incidence angle is kept constant at $\theta = 90°$. It is assumed that the droplet is of spherical shape prior to impingement, i.e. aerodynamic effects on the droplet geometry are being neglected. Therefore it is sufficient to incorporate only a short section of the flow path into the model, in the present case this length is 1.5 droplet diameters (1.5 d). The circular wall area around the impinging droplet is chosen to be 10 times the diameter of the droplet itself (10 d). These geometrical boundary conditions define a cylindrical computational domain of 3 d in height (including 0.5 d above initial droplet position) and 10 d in diameter. In order to limit the computational effort, only a 90° section of the domain with two orthogonal symmetry planes is regarded (see Fig. 3).

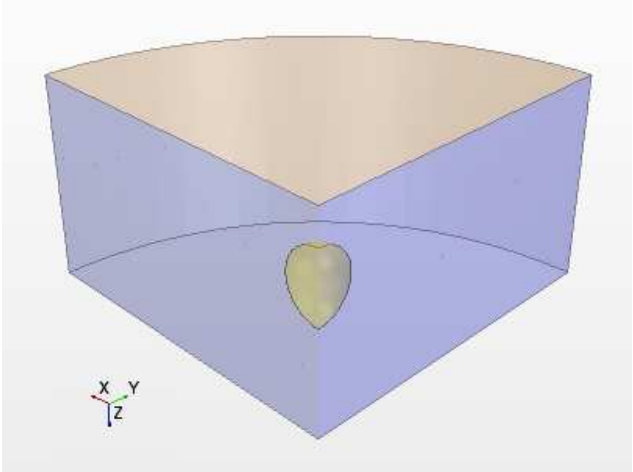

Fig. 3: Complete computational domain

The CFD software package employed for the analyses is STAR-CCM+ (v9.04.009). The mesh generator of this package allows to build 'trimmed hexahedral meshes'. The advantages of this mesh topology for the current investigation are the possibility of mesh alignment according to the main flow minimizing numerical diffusion and a high flexibility in local mesh refinement. The final computational mesh consists of 4.95 million cells with a highest refinement in the droplet flow path and 1d above the wall. The edge lengths of the cells in this region are 1/60 d. A top view of the central refinement area of the mesh is shown in Fig. 4.

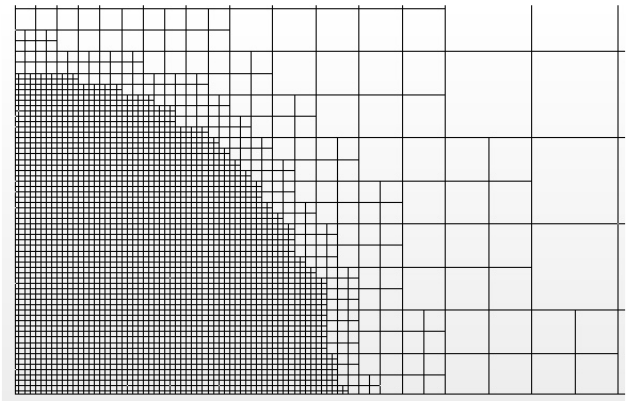

Fig. 4: Top view of computational mesh (refinement area of droplet flow path)

The numerical analyses are performed as implicit unsteady turbulent VOF analyses including surface tension effects. Second order differencing in space, first order differencing in time and realizable k-epsilon turbulence modelling are applied. Initial conditions are zero velocity in the air volume and the respective droplet velocity in the droplet volume. Although the liquids in the technical application exhibit non-Newtonian behaviour the analyses covered in this paper are performed assuming constant thermophysical properties since the

development of the final rheological model for the complete process will be based upon the results presented here. The gaseous phase in all simulations is air at ambient temperature and pressure.

In order to achieve the Courant number criterion of Co < 1 time steps are defined for each analysis individually, resulting e.g. in a time step size of $8x10^{-10}$ sec for a droplet diameter of 100 µm and an initial droplet velocity of 80 m/s. The analyses are terminated when the volume-averaged shear rate in the liquid phase monitored during the analysis is reduced by 10% after reaching a maximum.

VALIDATION OF NUMERICAL SETUP

A validation of the numerical setup including mesh resolution, differencing schemes and time step size is required in order to guarantee physically meaningful results regarding the shear rates during the droplet-wall interaction process. Since no own experimental work in this context is available the simulations need to be validated against adequate literature data. It was decided to use the Bai-Gosman model [7] as a standard against which to review the results of the own analyses. This model predicts the outcome of a droplet-wall interaction and proposes 6 possible regimes as functions of Weber number, Laplace number and wall temperature range. For the temperature range of interest, i.e. a wall temperature below the saturation temperature of the droplet, 4 regimes can be distinguished:

- Droplet adheres to wall (We < 2)
- Droplet rebounds from wall (2 < We < 20)
- Droplet spreads on wall (20 < We < We_c)
- Droplet splashes (We > We_c)

The critical Weber number We_c is defined as

$$We_c = A \cdot La^{-0.18}$$

with the Laplace number

$$La = \rho \cdot \sigma \cdot d / \mu^2$$

and the splash onset coefficient A which defaults to A = 1320 for smooth walls and wetted rough walls.

The Laplace numbers according to the preliminary experimental investigation are 0.39 < La < 0.63, which delivers critical Weber numbers of 1434 < We_c < 1564. The droplet-wall interaction regime therefore generally is expected to be 'splash' in the technical application. For the validation of the numerical setup, the range of investigated Weber numbers is extended to include the regime 'spread' in some parameter combinations.

The results of a first series of analyses prove the validity of the basic numerical setup. During the flow of the droplet, the high mesh resolution and the small Courant numbers together with the HRIC discretization scheme for convection deliver satisfactorily sharp phase interfaces. No relevant effects of numerical diffusion can be detected. Due to the mainly convective transport of the phase volume fraction α_i and the very low velocities perpendicular to the wall in the first cell layers adjacent to an initially dry wall the phase volume fraction never reaches a value of 1 (corresponding to 100% liquid) in this mesh region during the complete impingement process. Since the thermophysical properties of the fluid are calculated as weighted averages of the physical properties of the constituent phases and their phase volume fractions, e.g.

$$\mu = \sum_i \mu_i \alpha_i$$

the viscosity of the fluid adjacent to the initially dry wall never reaches the value of the viscosity of the liquid phase. In consequence, the droplet will potentially exhibit a non-physical flow pattern during the droplet-wall interaction process since wall shear stress is reduced by the unrealistic viscosity in this area. In the first series of analyses even for Weber numbers much higher than We_c no splashing of the impinging droplet can be observed. Instead, the droplet spreads into a large number of radial filaments as shown in Fig. 5.

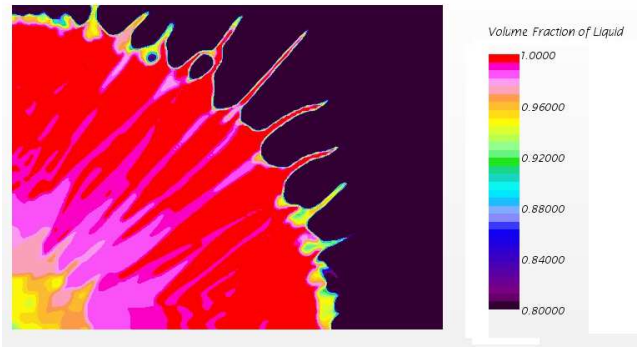

Fig. 5: Droplet spreading into filaments

In order to receive more realistic flow patterns either the local viscosity in the near-wall region has to be adjusted or the wall has to be covered by a thin liquid film. In [8], the influence of the wall film thickness in VOF analyses of droplet-wall interaction phenomena is investigated and compared to experimental data. For thin films of δ < d the film thickness has only a minor influence upon the overall droplet-wall interaction process. In the present investigation the minimum required film thickness to achieve a splash regime is found to be δ = 0.05 d. Based upon this finding, the benchmark of the VOF simulations against the Bai-Gosman model is performed with an initial liquid film of 0.05 d thickness on the wall. This procedure is in agreement with the Bai-Gosman model, since the default value of the splash onset coefficient A can be applied for both smooth dry and for wetted walls.

The simulations are performed following the setup described above with water under ambient conditions as the

droplet and film liquid and the initial conditions as given in Tab. 1.

Droplet diameter	Initial droplet velocity	Droplet Weber number	Bai-Gosman regime	Observed regime in CFD
[mm]	[m/s]	[-]		
0.06	8	52	spread	spread
0.06	60	2912	splash	splash
0.06	100	8088	splash	splash
0.1	8	86	spread	spread
0.1	60	4853	splash	splash
0.1	100	13481	splash	splash

Tab. 1: Comparison of droplet-wall interaction regimes

Typical results for the phase distribution during the droplet-wall interaction process are shown in Figs. 6 (spread) and 7 (splash). In both cases the droplet impinging on the thin liquid film generates a ring-shaped wave traveling in radial direction with the velocity decreasing over time.

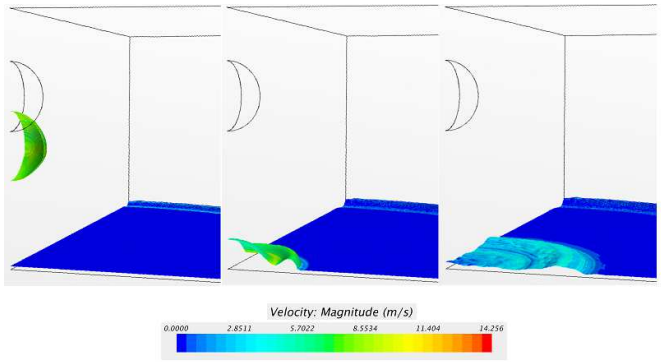

Fig. 6: Droplet-wall interaction in spread regime (We = 86)

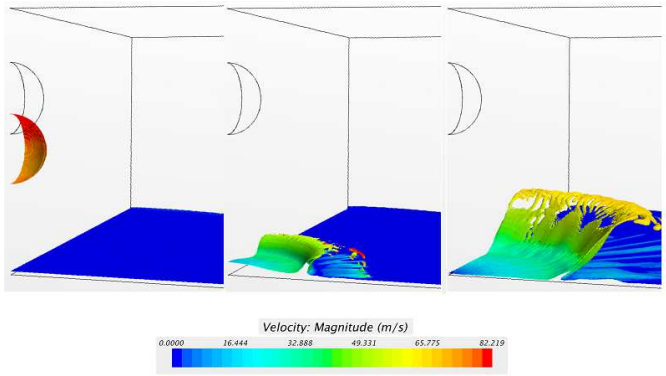

Fig. 7: Droplet-wall interaction in splash regime (We = 4853)

While in the spread regime the wave shape remains roughly sinusoidal in cross section, the higher momentum transfer between impinging droplet and film in the splash regime causes the wave to steepen considerably and subsequently to be fragmented into droplets. The limited mesh resolution at larger distances from the wall does not allow to capture the fragmentation process in detail.

Available hardware resources limit the number of validation analyses to the list given in Tab. 1. Although the precise Weber numbers for the areas of transition between the individual droplet-wall interaction regimes are not reproduced, it can be concluded that the setup of computational domain and numerical schemes delivers simulation results that are in accordance with the Bai-Gosman model for droplet-wall interaction. Consequently the setup should be adequate to deliver realistic values for the shear rates occurring during the process.

RESULTS FOR TRANSIENT SHEAR RATES

For the investigation of the transient shear rates occurring during the droplet-wall interaction the list of analyses given in Tab. 1 is expanded to a total of 24 simulations covering 3 droplet diameters, 4 droplet initial velocities and 2 sets of thermophysical properties (water and paraffin, thermophysical properties in Tab. 2). The choice of substances is justified by the desired comparability against a broad data base (water) and the selection of a Newtonian fluid with properties close to the process fluids of the technical application (paraffin).

		water	paraffin
Density	[kg/m³]	998	1030
Dyn. Viscosity	[Pas]	0.889E-03	2.0E-03
Surf. Tension	[N/m]	0.074	0.0463

Tab. 2: Thermophysical properties of liquid phase

The transient shear rates are calculated as the instantaneous volume-average of the magnitude of the velocity gradient in the liquid phase. A typical plot of the transient shear rate vs. time in a splash regime is given in Fig. 8.

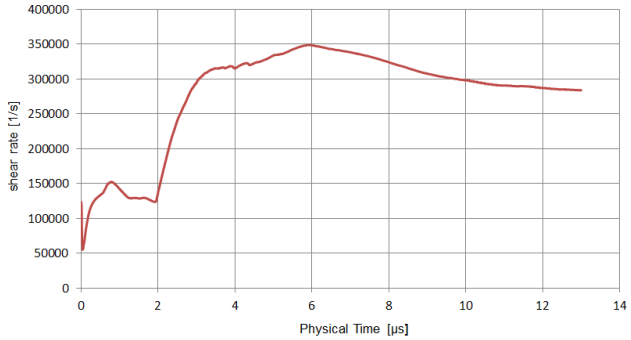

Fig. 8: Transient shear rate vs. time

During the first 2 µs the droplet is in free flight and a constant transient shear rate develops. This shear rate is non-zero due to the velocity gradients at the droplet surface and due to local perturbations at the liquid film surface that are mainly

numerical artefacts. When the droplet impinges, the transient shear rate increases rapidly and in his case reaches a maximum of 350000 1/s after 6 µs. At this time, the droplet has already completely spread and the ring wave starts to fragment. Subsequently the transient shear rate decreases gradually. The overall curve looks very similar in the spread regime with a lower maximum value, however. All results of the maximum transient shear rates are collected in Figs. 9 and 10.

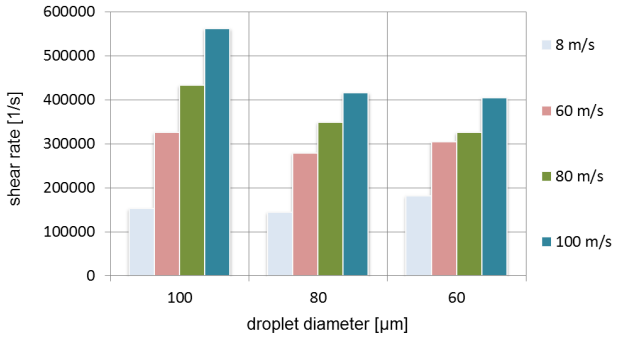

Fig. 9: Maximum transient shear rates (water)

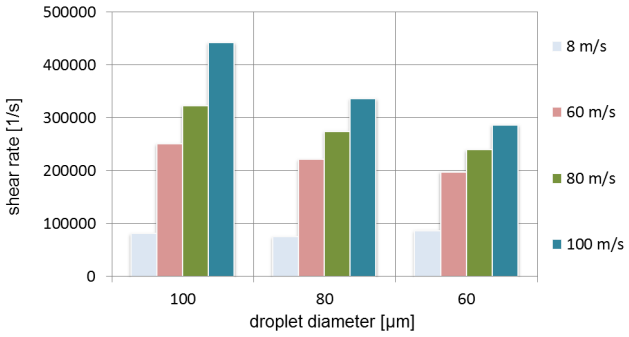

Fig. 10: Maximum transient shear rates (paraffin)

DISCUSSION AND CONCLUSIONS

The results of the numerical analyses demonstrate considerable shear rates of up to 560000 1/s in the droplet and the liquid film during the process of droplet-wall interaction. As physically feasible, larger droplet velocities and larger droplet diameters generate higher shear rates. With the thermophysical properties of paraffin, the obtained shear rates are lower compared to the data obtained with water due to the higher dynamic viscosity of paraffin limiting the velocity gradients in the process. As such, the performed investigations can be judged as very successful with respect to both the prediction of the physical process itself (comparison with Bai-Gosman model) and the application of the VOF methodology to produce physically meaningful transient shear rates in droplet-wall interaction. The obtained data in a next step will be incorporated into an overall rheological model of the technical process to improve the prediction quality of corresponding analyses.

However, a few open questions still exist that will have to be addressed. On the numerical side, there is some uncertainty regarding the absolute value of the obtained transient shear rates due to the observed random velocity perturbations on the liquid film surface which are a standard problem in VOF analyses. These can be regarded as 'numerical noise' and interfere with the desired shear rate data from the main droplet-wall interaction process. It will be the main object of a next step in the numerical investigation to either minimize the perturbations or to exclude them from the averaging process to obtain the transient shear rates. Regarding the overall technical process of automobile body conservation only after the implementation of the full rheological model will it be possible to quantify the influence of the high-shear condition during the impingement of the droplet on the wall or liquid film with respect to the overall liquid film behavior. This mainly depends upon the time constants of the viscosity changes following a step change in shear condition e.g. from high-shear to almost zero shear in the nozzle and back to high-shear during droplet-wall interaction. These time constants have to be determined experimentally and will be included in the rheological model. Unfortunately, measuring these time constants is a non-trivial task even for experienced experimentalists. Additional activities to be performed in the overall project will be a further expansion of the Weber number range to validate the methodology also for the two remaining Bai-Gosman regimes of 'rebound' and 'adhere' and a further refinement of the computational domain in order to investigate the fragmentation process of the ring wave in more detail. In this context it may also be necessary to re-discuss and evaluate the influence of the numerical setup on the phenomenology of the process.

REFERENCES

[1] Rother, K., Steinbeck-Behrens, C., Kern, S.: Towards a Virtual Process Chain for Body Painting – Modular Developments and Implementation Strategies. *Proceedings of the 3rd Intl. Strategy Conference "Core Issues for Future Car Body Painting", Berlin,* June 2002.

[2] Scheibe, A., Westkämper, E., Ye, Q.: Numerical Simulation of Painting Processes. *Proceedings of NAFEMS Seminar "Simulation of Complex Flows (CFD) – Applications and Trends", Wiesbaden,* March 2008.

[3] Herschel, W.H., Bulkley, R.: Konsistenzmessungen von Gummi-Benzollösungen. *Kolloid-Zeitschrift* 39, 1926, pp. 291-300.

[4] Barnes, H.A.: Thixotropy – A Review. *J. Non-Newtonian Fluid Mech.* 70, 1997, pp. 1-33.

[5] Hirt, C.W., Nichols, B.D.: Volume-of-Fluid Methods for the Dynamics of Free Boundaries. *J. Computational Physics* 39, 1981, pp. 201-225 .

[6] Muzaferija, S., Peric, M.: Computation of Free Surface Flows using Interface-Tracking and Interface-Capturing Methods. *Nonlinear Water Wave Interaction*. Computational Mechanics Publications, WIT Press, Southampton, 1999.

[7] Bai, C., Gosman, A.D.: Development of Methodology for Spray Impingement Simulation. *SAE Technical Paper Series* 950283.

[8] Nikolopoulos, N., Theodorakakos, A., Bergeles, G.: Normal impingement of a droplet onto a wall film: a numerical investigation. *Int. J. of Heat and Fluid Flow* 26 (2005), pp. 119–132